Design and Validation of Compact Antenna Test Ranges using Computational EM

O. Borries, P. Meincke, E. Jørgensen,
H.-H. Viskum, F. Jensen
TICRA
Copenhagen, Denmark
ob@ticra.com

C. H. Schmidt
Airbus Defence & Space
Munich, Germany
carsten.schmidt@airbus.com

***Abstract*—The design of modern Compact Antenna Test Ranges (CATRs) is a challenging task, and to achieve strong performance, simulation using computational electromagnetics is a vital part of the design process. However, the large electrical size, geometrical complexity and high accuracy requirements often mean that the available computer resources are not sufficient for running the simulation. In the present paper, we highlight some recent developments that allow for much larger, faster and more accurate simulations than was possible just a few years ago, and apply them to realistic ranges. The conclusion is clear: Modern software tools allow designers of CATRs to achieve better performance in shorter time than was previously possible.**

I. Introduction

The task of finding the far-field characteristics of an antenna can be completed using a variety of techniques, including software modelling, small-scale models and real-life testing of a full-size system in an antenna test range. In practice, while a combination of these approaches are typically used in various stages of the design process, the use of an antenna test range is ubiquitous, particularly in the last stage of the design where validation of the system is necessary. The obtained measurements can then be compared to specifications and/or numerical simulations.

For far-field measurements, a Compact Antenna Test Range (CATR) is a common alternative to the outdoor far-field ranges, allowing an indoor and fairly compact measurement range. The key feature of a CATR is the Quiet-Zone (QZ) it produces, which is a region in which the field behaves like a plane wave: with uniform amplitude and phase and with very low cross-polarization. However, the design of a CATR is no easy task. In particular, there is a large number of design variables to adjust when attempting to get optimum performance.

Facing strict requirements on the total size of the configuration and quality of the QZ, quantities that are inversely proportional, the design and analysis phase of a CATR design is very demanding and often requires the use of Computational Electromagnetics (CEM) as a simulation tool. Unfortunately, with the large bandwidth requirements and complicated geometry, simplifications are often necessary to run the simulations within acceptable time frames [1], [2], [3]. Judging the impact of these simplifications on the final results requires a great deal of experience, and can be a barrier for achieving the target performance of a system. There is great interest in using CEM to optimize various aspects of a CATR design [4], [2], [5], but one of the main problems has been the time required for the analysis.

In the present paper, we consider some recent developments in CEM and show how they allow much faster and more accurate CATR simulations than were previously possible. Beginning with a general discussion of the developments, with emphasis on their benefits for CATR design, we then illustrate the performance by performing a few parameter sweeps. Finally, we address the most important concern regarding the use of CEM in the design phase of an actual system, namely validation of the results, by comparing the simulated results against measurements of a CATR system from Airbus Defence & Space.

II. Analysis Methods

There are three main approaches for analysing CATRs, depending on the required accuracy and electrical size of the system.

A. Geometrical Optics

Geometrical Optics (GO), possibly including diffraction by means of Uniform Theory of Diffraction (UTD), has previously been a common analysis tool for CATR, particularly when attempting to optimize the system [4]. With the progress in computing power and CEM algorithms, it appears to be used less frequently, at least for the later stages of the design process. However, it still has several key features that justify its use in CATR design:

- Strictly speaking, its time and memory requirements are independent of the frequency. As such, for extreme electrical sizes, it can be the only option.
- By disregarding UTD and only tracing reflected rays, GO can allow users to gauge the ”ideal” performance of the system, i.e. if no diffraction was present. This approach has been used in the literature [6], and can allow more efficient optimization by subtracting the feeds amplitude taper from the quiet zone performance, isolating the amplitude ripples due to diffraction.

B. Physical Optics/PTD

A very popular algorithm for the analysis of CATRs, and reflectors in general, is Physical Optics (PO), combined with Physical Theory of Diffraction (PTD) [5]. While still an asymptotic method, like GO/UTD, it is very accurate for large, smooth structures. Unfortunately, it is typically much more time-consuming than GO/UTD, in particular for dual-reflector CATR because one typically needs to compute multiple interactions between the sub- and main reflectors.

For Physical Optics on electrically large structures, GRASP is often recognized as an industry leading tool, due to its use of customized sparse integration rules which reduce the number of samples of the integrand, resulting in much faster computation. However, the main caveat of PO remains: The computational time generally scales as $\mathcal{O}(f^4)$, where f is the frequency, such that doubling the frequency means that the computation takes 16 times longer. To reduce this scaling, there has been a large effort in recent years to develop accelerated algorithms, also called "fast" algorithms, that reduce the scaling of PO to $\mathcal{O}(f^2 \log f)$, similar to how the FFT reduces the scaling of the discrete Fourier transform. While some "Fast-PO" algorithms were published in the last decade, it was only recently [7] that algorithms were presented that provided both sufficient speed-up and accuracy to allow their use in the design of high-accuracy systems such as a modern CATR. In GRASP 10.4, these algorithms have been implemented.

Figure 1 shows the time consumption compared between GRASP 10.3 and GRASP 10.4 for a scenario where a $1\,\mathrm{m} \times 1\,\mathrm{m}$ plate is illuminated by a plane wave at oblique incidence, and its forward hemisphere near-field is computed at a radius of $0.8\,\mathrm{m}$ from the center of the plate. By increasing the frequency, and thus the electrical size of the plate, we can see that the algorithm indeed provides roughly the expected reduction in scaling. Further, as illustrated by the Relative RMS error curve, the accuracy is fully maintained throughout the frequency range. It is worth noting that the algorithm requires no user intervention - it is activated automatically if beneficial, and all relevant parameters are adjusted as needed by the program.

Furthermore, performing PTD on a CATR can be cumbersome for an entirely different reason: Since the serrations are attached to the CATR, GRASP 10.3 users are required to manually select the edges where PTD should be included to avoid computing PTD on internal edges. This is time-consuming and error-prone. In GRASP 10.4, an automatic edge/wedge detection algorithm has been implemented, such that GRASP only includes PTD contributions from external edges.

C. Method of Moments

Method of Moments (MoM) is a full-wave method, meaning that it takes into account all physical phenomena. It works by discretizing the surface of the object using geometrical patches, and then represents the current on those patches using polynomial vector basis functions. MoM is accurate; the expected dynamic range of the implementation in GRASP

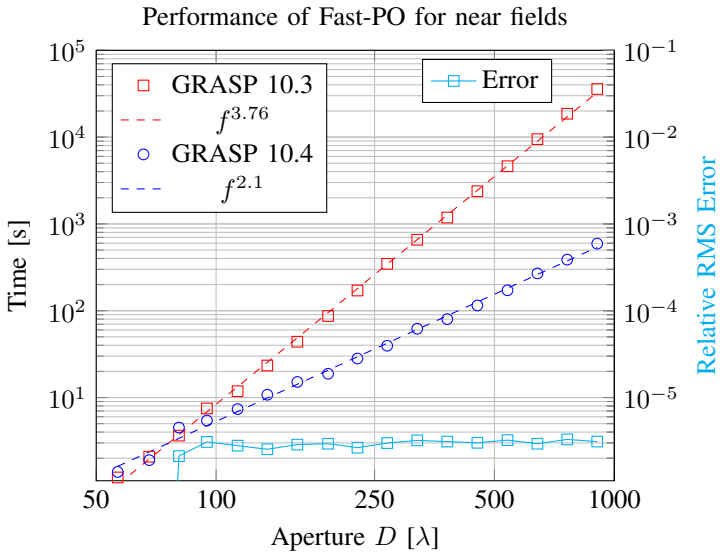

Fig. 1. Performance of the Fast-PO implementation in GRASP 10.4 for near fields compared to the direct PO implementation in GRASP 10.3. The Relative RMS Error between the fields obtained from direct PO and Fast-PO is shown in cyan.

is about 60 dB for the default accuracy, and the accuracy can be further improved if requested by the user. Since it takes into account all phenomena, but requires $\mathcal{O}(f^4)$ scaling of memory and computational time, it is typically used only on small-scale or simplified CATR models.

MoM can be accelerated by the Multi-Level Fast Multipole Method (MLFMM), which has $\mathcal{O}(f^2 \log f)$ scaling. MLFMM was implemented recently in GRASP, and was adapted to the efficient Higher-Order (HO) basis functions used in GRASP, which allow much lower memory requirements [8], [9] than implementations based on Rao-Wilton-Glisson (RWG) basis functions.

An annoying detail when creating meshes of the geometry is the need for continuity in the mesh. This means that when combining two different meshes, say, a mesh of the main reflector combined with the mesh of the serrations, great care must be taken to ensure that the patches are continuous, such that current is allowed to flow between the patches.

In GRASP 10.4, this has been greatly simplified by automatically joining meshes that are connected, even if the patches are not continuous [10]. This allows users to remesh the complicated parts of the geometry, e.g. the serrations, without being forced to consider connectivity.

III. Examples

In the following, we consider some CATR configurations, illustrating how CEM can help in the design and analysis of such a system. The designs are not meant as a suggestion for an ideal CATR design, but as representative examples to illustrate the speed, accuracy and efficiency of using the various CEM algorithms outlined in the previous section.

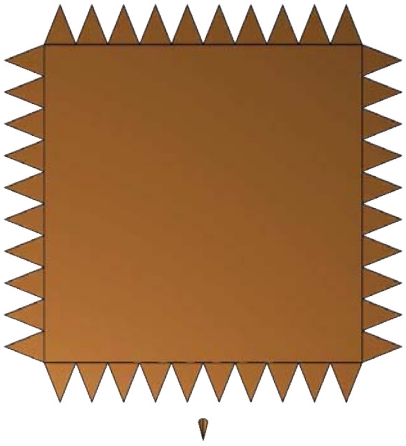

Fig. 2. Illustration of the offset single reflector system with rectangular rim and serrations.

Unless otherwise mentioned, the calculations are performed using GRASP 10.4 on a standard laptop with 16 GB memory and a 2.6 GHz Intel Core i7.

A. Single reflector with serrations

As a first example, we consider a single offset reflector system at 30 GHz. The main reflector is a square reflector of edge length L meters when projected onto a plane orthogonal to the beam axis, excluding the ten serrations on each side. Each serration is triangular and protrudes S meters from the reflector, and the total size of the reflector is 1×1 meter. Thus, we require that $L + 2S = 1$. The focal length of the system is 1.5 meter, and the clearance between the feed and the lowest part of the serrations is 5 cm. There are 10 serrations along each side, such that the width of each serration is $L/10$ at the base. The feed is modelled as a Gaussian Beam, with a taper of -3 dB at the tip of the serrations. The quiet zone is $0.5\,\mathrm{m} \times 0.5\,\mathrm{m}$, and is located 2.05 meter in front of the centerpoint of the reflector. A sketch of the design is shown in Figure 2. We note that the serrations are isosceles triangles, and thus diffractions from the serrations at the corners of the reflector will significantly disrupt the quiet zone.

As a first step, we compare the results obtained by MLFMM with that obtained by PO/PTD, shown in Figure 3 for $S = 0.1$. The sampling density of the field is $\lambda/5$, resulting in a quiet-zone grid of 251×251 points. The correspondence is very good, with the deviations below -80 dB, justifying the use of the much faster PO/PTD (8.5 sec) instead of the more costly MLFMM (5:31 min, 2.5 GB). Interestingly, the PO time is roughly an order of magnitude lower than for GRASP 10.3, which did not apply Fast-PO and thus required 87 seconds for PO/PTD. For the full-wave simulation, GRASP 10.3 did not include MLFMM and thus required 204 GB of memory for an unaccelerated MoM solution.

The fast and accurate analysis demonstrated in this scenario opens up a wide range of possibilities for design optimization. In particular, optimization of serrations has been considered

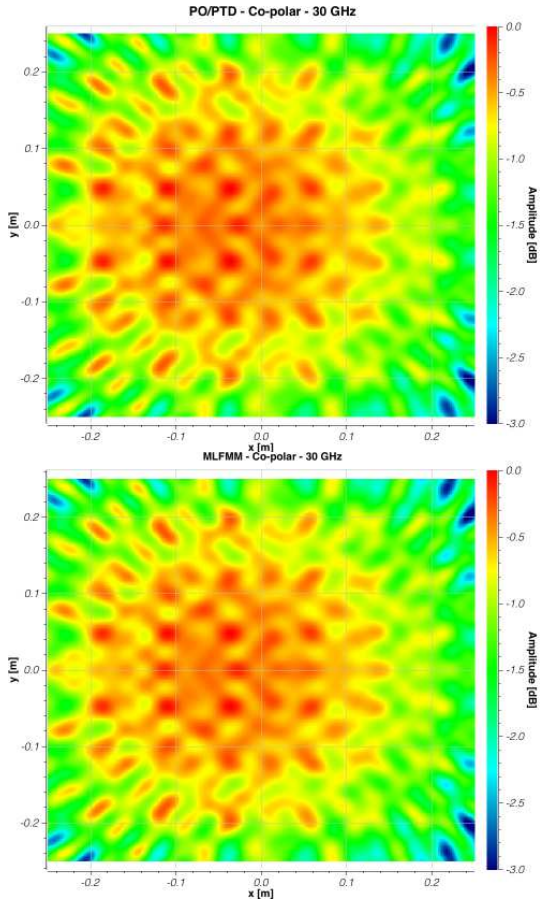

Fig. 3. Comparison between PO/PTD and MLFMM in the quiet zone.

previously on small-scale models [4], [3], but these works required either

- simplifying the geometry, and/or
- considering only electrically small structures, and/or
- using GO/UTD.

However, with the recent advances discussed in the previous section, optimization of actual CATRs at realistic frequencies is possible with full-wave analysis methods. Actual use of optimization is outside the scope of the present paper, but to illustrate the efficiency, Figure 4 shows how the length of the serrations relative to the total size of the system can be adjusted. The figure is a sweep across 50 values of S between 0.01 and 0.25, remembering that the total sidelength of the system $L + 2S$ is kept fixed at 1 meter. As a quality estimate of the Quiet Zone, we use the following measure:

$$\text{Quality} = \frac{1}{N_s} \sum_{i=1}^{N_s} |E_i - M|^2, \tag{1}$$

where E_i is the co-polar component from the PO/PTD analysis. $M = \frac{1}{N_s} \sum E_i$ is the average of the co-polar field across all N_s sample points.

We remark that this quality estimate is very dependent on the taper of the feed, and thus cannot be used to compare the quality of quiet zones provided by different feeds. However, it

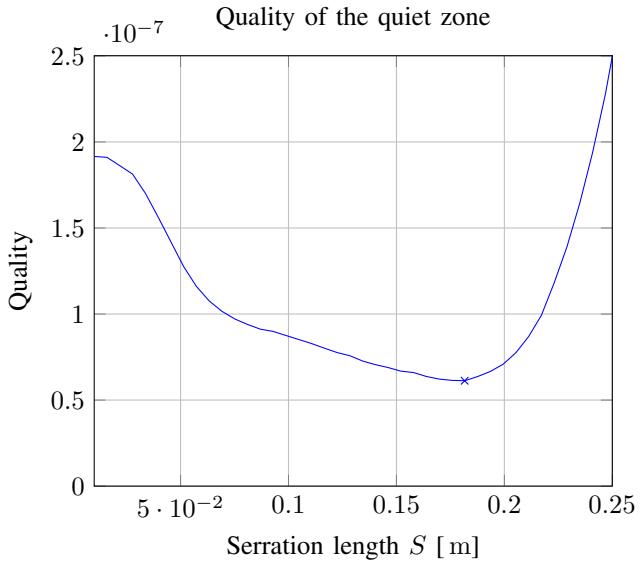

Fig. 4. Quality of the quiet zone relative to the length of the serration length. The 'x' marks the minimum of the curve.

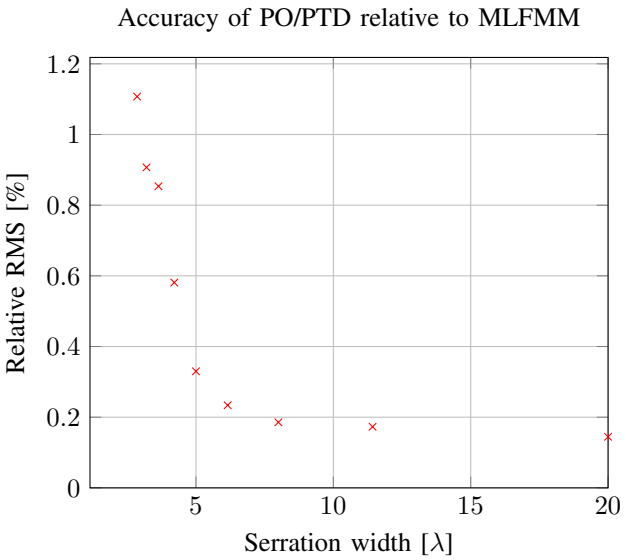

Fig. 5. Accuracy of PO/PTD as a function of serration width. The serration length is 10λ.

allows a simple quantification, suitable for parameter sweeps or even optimization of the geometry. The sweep is completed in about 6 minutes.

However, when analysing the serrations, it is important to keep in mind the limitations of PO/PTD. While larger serrations are excellently approximated by PO/PTD, the accuracy is reduced if small and/or geometrically complicated serrations are considered.

To illustrate this, in Figure 5, we adjust the electrical width of the serrations at the base, for S fixed at $S = 0.1\,\mathrm{m}$, and computes the Relative RMS between PO/PTD and MLFMM. The Figure contains a discrete set of points, as only those serration widths that allow the reflector edges to be completely covered by the serrations are considered. In other words, L divided by the serration width is required to be an integer. As expected, PO/PTD provides excellent agreement for the wide serrations but deteriorates to more than 1% once the serration width is below 2.5λ. Note, however, that even when the serrations are electrically small and/or geometrically complicated, PO/PTD can still be very useful as a first stage in an optimization.

B. Validation

To validate the performance against measurements, we consider a dual reflector compensated serrated CATR, the CCR 75/60, from Airbus Defence & Space, one of the leading manufacturers of compensated compact ranges. The general setup of the system is shown in Figure 6 and Figure 7. The main reflector is $7.5\,\mathrm{m} \times 6.0\,\mathrm{m}$, yielding a cylindrical quiet zone with a 5 meter diameter. The geometry of the serrations is quite complicated, and its implementation in GRASP was discussed in detail in [5].

For the purpose of the validation, the probing measurements were done at $4.2\,\mathrm{GHz}$ and $12.0\,\mathrm{GHz}$ with standard gain horns

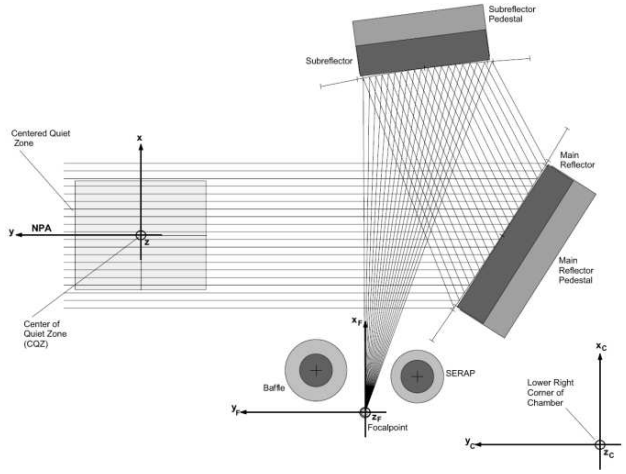

Fig. 6. Geometry of the CATR and the measurement planes.

Fig. 7. Picture of the CCR 75/60 system.

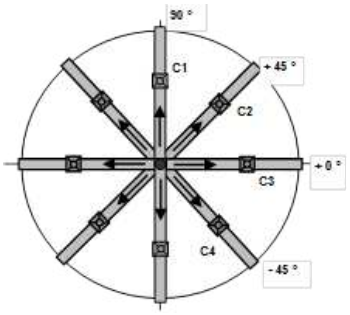

Fig. 8. Cuts in the QZ, as seen from the main reflector. Thus, the cut C3 corresponds to a movement along the x axis, with y and z fixed.

from Narda. The global coordinate system $(x_{\mathrm{F}}, y_{\mathrm{F}}, z_{\mathrm{F}})$ is placed at the feed, with the x-axis going from feed to the sub reflector and y-axis going to the QZ. The center of the QZ coordinate system is $(x, y, z) = (8.0895\hat{\mathbf{x}}_{\mathrm{F}}, 10.2480\hat{\mathbf{y}}_{\mathrm{F}}, 0)\,\mathrm{m}$. The probing was done in the x, z plane, with $y = -2.484\,\mathrm{m}$ at $4.2\,\mathrm{GHz}$ and $y = -2.216\,\mathrm{m}$ at $12.0\,\mathrm{GHz}$. Four cuts through the QZ were measured, as specified in Figure 8.

To perform computations on this system, we begin by applying Physical Optics and compute the nominal path through the system:

1) Feed illuminates sub reflector.
2) Sub reflector illuminates main reflector.
3) Sub- and main reflectors illuminate QZ.

This computation takes a few minutes, and allows a quick overview of the performance of the system. In particular, since this analysis does not include any multiple interactions, the result can be compared with the measurements to illustrate where in the QZ such multiple interactions are most significant.

Following the initial Physical Optics results, we now turn to full-wave simulations. As shown in the schematic of the CATR setup, the system also includes two absorbing structures, a SERAP (to reduce illumination of the main reflector by the feed) and a baffle (to reduce illumination of the QZ by the feed). While these structures can be fully included in the simulation, their geometry is quite complicated - instead, we simply remove the mentioned contributions from the simulation. Hence, the simulation order is:

1) Feed illuminates sub reflector.
2) Sub reflector illuminates main reflector.
3) Main reflector back scattering onto sub reflector.
4) Sub reflector back scattering onto main reflector.
5) Sub- and main reflector illuminates QZ.

Thus, the simulation takes into account up to third order interactions between the sub- and main reflectors. All computations are done by applying MLFMM. To illustrate the footprint of the main reflector, and the complicated mesh that follows, the mesh of the main reflector is shown in Figure 9. The simulation at $4.2\,\mathrm{GHz}$ requires roughly 7.4 GB of memory and about 47 minutes of simulation time on a modest computing server, with 2 Intel Xeon E5-2690 and 160 GB memory.

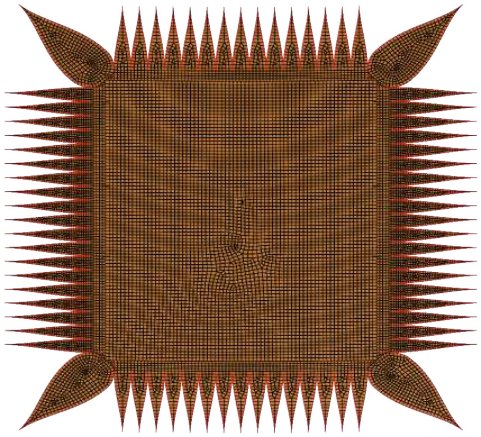

Fig. 9. Mesh of the main reflector.

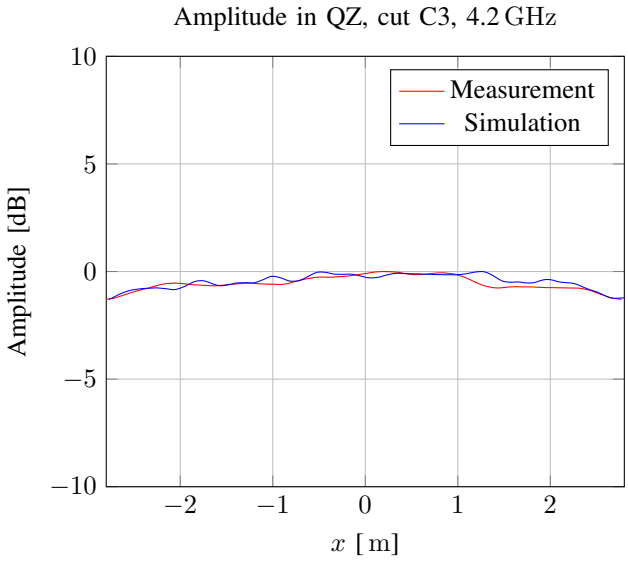

Fig. 10. Comparison between GRASP MLFMM and measurement at $4.2\,\mathrm{GHz}$ of the Airbus CCR 75/60, amplitude.

Considering the C3 cut along the x axis, the results are shown in Figures 10-11 for the amplitude and phase, respectively. We see a strong agreement between the measurement and simulation in amplitude, in spite of the simulation not applying probe correction and not fully simulating the SERAP and baffle absorbing structures as well as the effects of the measurement chamber. The slightly poorer agreement for the phase than for the amplitude is primarily due to not simulating the absorbing structures, and the lack of interactions between the sub- and main reflector of higher than third order.

To further validate the simulations, we apply the same procedure for the range at $12.0\,\mathrm{GHz}$. The results are shown in Figures 12-13, and show an even stronger correspondence. However, the simulation time increases significantly, to 13 hours and with a peak memory consumption of 41 GB, on the mentioned computing server. There are 3.5 million HO unknowns on the sub reflector and 4.3 million HO unknowns

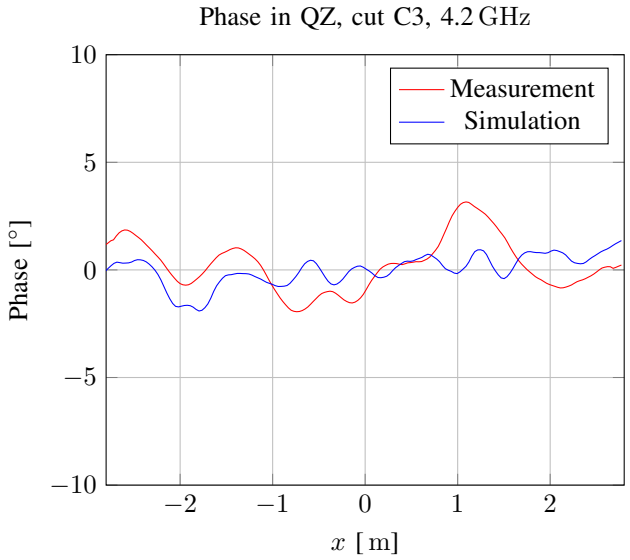

Fig. 11. Comparison between GRASP MLFMM and measurement at 4.2 GHz of the Airbus CCR 75/60, phase.

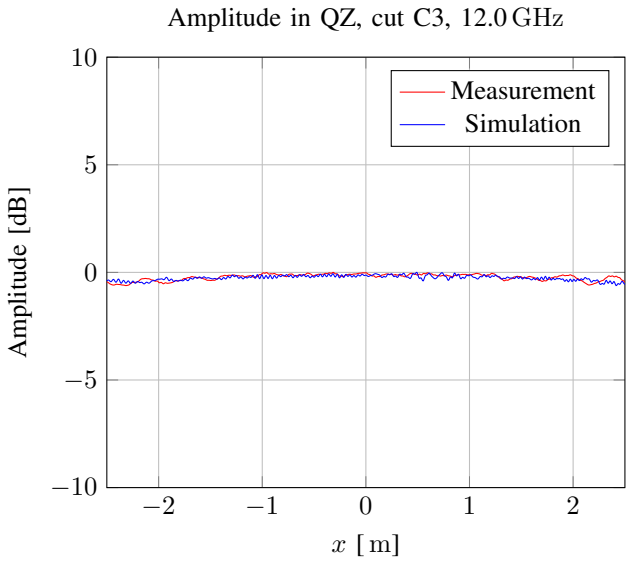

Fig. 12. Comparison between GRASP MLFMM and measurement at 12.0 GHz of the Airbus CCR 75/60, amplitude.

on the main reflector, corresponding to roughly 14 and 17 million RWG unknowns, respectively.

IV. Conclusion

In the present paper, we have described some recent developments in computational electromagnetics as implemented in GRASP 10.4, and shown how they have significantly expanded the range of solvable problems, even on modest computing platforms. In particular, we have described how they can be used to drastically reduce the simulation time required for CATR designs, allowing parameter sweeps and even small-scale optimization on CATRs that are too large to have been analyzed, let alone optimized, just a few years ago. Finally,

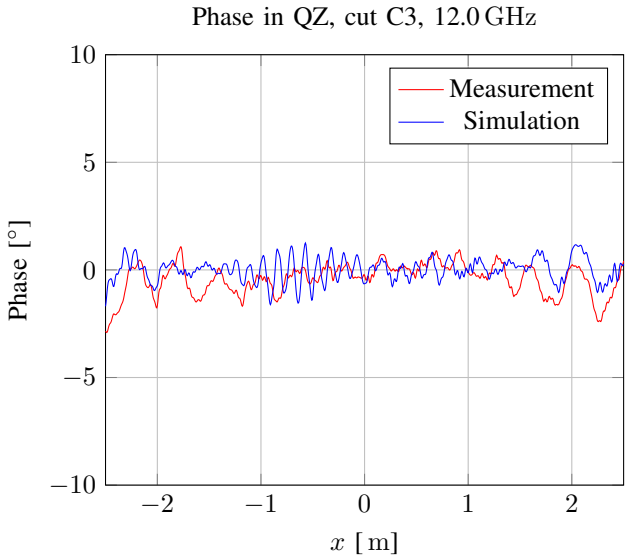

Fig. 13. Comparison between GRASP MLFMM and measurement at 12.0 GHz of the Airbus CCR 75/60, phase.

we have validated the accuracy on a complicated and realistic geometry, and shown that the simulations on a subset of the actual geometry provide an accurate description of the field in the quiet zone.

References

[1] K. Pontoppidan and P. H. Nielsen, "Guidelines for the Design of the Serrations of a Compact Range," in *PROCEEDINGS OF ISAP*, Fukuoka, Japan, 2000, pp. 1–4.

[2] J. Hartmann and D. Fasold, "Advanced Serration Design for Compact Ranges with UTD," in *Antenna Measurement Techniques Association*, Philadelphia, USA, 2000, pp. 1–6.

[3] F. Jensen, "Polarisation Dependent Scattering from the Serrations of Compact Ranges," in *Antenna Measurement Techniques Association*, Nov. 2007, pp. 150–155.

[4] J. Hartmann and D. Fasold, "Improvement of Compact Ranges by Design of Optimized Serrations," in *Millenium Conference on Antennas and Propagation*, Davos, Switzerland, 2000, pp. 1–4.

[5] C. H. Schmidt, A. Geise, J. Migl, H.-J. Steiner, and H.-H. Viskum, "A Detailed PO/PTD GRASP Simulation Model for Compensated Compact Range Analysis with Arbitrarily Shaped Serrations," in *Antenna Measurement Techniques Association*, Oct. 2013, pp. 6–11.

[6] I. J. Gupta, K. P. Ericksen, and W. D. Burnside, "A Method to Design Blended Rolled Edges for Compact Range Reflectors," *IEEE Transactions on Antennas and Propagation*, vol. 38, no. 6, pp. 853–861, Jun. 1990.

[7] O. Borries, H. H. Viskum, P. Meincke, E. Jørgensen, P. C. Hansen, and C. H. Schmidt, "Analysis of Electrically Large Antennas using Fast Physical Optics," in *European Conference on Antennas and Propagation*, Lisbon, Portugal, Apr. 2015.

[8] E. Jørgensen, J. Volakis, P. Meincke, and O. Breinbjerg, "Higher Order Hierarchical Legendre Basis Functions for Electromagnetic Modeling," *IEEE Transactions on Antennas and Propagation*, vol. 52, no. 11, pp. 2985–2995, Nov. 2004.

[9] O. Borries, P. Meincke, E. Jørgensen, and P. C. Hansen, "Multilevel Fast Multipole Method for Higher-Order Discretizations," *IEEE Transactions on Antennas and Propagation*, vol. 62, no. 9, pp. 4695–4705, Sep. 2014.

[10] Z. Peng, K.-H. Lim, and J.-F. Lee, "A Discontinuous Galerkin Surface Integral Equation Method for Electromagnetic Wave Scattering From Nonpenetrable Targets," *IEEE Transactions on Antennas and Propagation*, vol. 61, no. 7, pp. 3617–3628, Jul. 2013.